Key Points:
- We present a detailed stable isotopic and Mg/Ca record for the early Eocene-Oligocene transition from southern Australia at ~51°S
- Shallow shelf (<100 m deep) seawater temperatures fell 2 °C across this part of the transition
- Surface seawater δ18O values were probably closer to positive one than negative one within this embayment in the latest Eocene, indicating that a source of relatively saline water was present at this time

Midlatitude Southern Hemisphere Temperature Change at the End of the Eocene Greenhouse Shortly Before Dawn of the Oligocene Icehouse

A. M. Haiblen[1,2] [ID], B. N. Opdyke[1] [ID], A. P. Roberts[1] [ID], D. Heslop[1] [ID], and P. A. Wilson[3] [ID]

[1]Research School of Earth Sciences, The Australian National University, Canberra, Australia, [2]Now at Geoscience Australia, Symonston, Australia, [3]National Oceanography Centre Southampton, University of Southampton, Southampton, UK

Abstract The Eocene-Oligocene transition (EOT) marked the initiation of large-scale Antarctic glaciation. This fundamental change in Cenozoic climate state is recorded in deep-sea sediments by a rapid benthic foraminiferal $\delta^{18}O$ increase and appearance of ice-rafted debris in the Southern Ocean. However, we know little about the magnitude of cooling associated with the EOT in shallow water environments, particularly at middle to high latitudes. Here we present new stratigraphic records of the C13r/C13n magnetochron boundary and the EOT in the clay-rich Blanche Point Formation, South Australia. The Blanche Point Formation was deposited in a shallow shelf setting (water depths of <100 m) at a paleolatitude of ~51°S. We present high-resolution $\delta^{18}O$, $\delta^{13}C$, and Mg/Ca records of environmental change from well-preserved benthic foraminifera of latest Eocene age at this site. A marked, negative $\delta^{13}C$ excursion occurs immediately before EOT Step 1 and may be a globally representative signal. An ~2 °C cooling of shallow shelf seawater is evident from benthic foraminiferal Mg/Ca across Step 1. This cooling signal is both sufficient to account fully for the $\delta^{18}O$ increase in our data and is of similar amplitude to that documented in published records for shallow shelf and upper water column open ocean settings, which suggests no obvious polar amplification of this cooling signal. Our results strengthen the evidence base for attributing EOT Step 1 to global cooling with little contribution from ice volume growth and contradict the mechanism suggested to explain the inferred northward migration of the intertropical convergence zone in the contemporaneous equatorial Pacific Ocean.

1. Introduction

The Eocene-Oligocene transition (EOT) marked the onset of sustained, large-scale Antarctic glaciation and the Cenozoic transition from a "greenhouse" to an "icehouse" world (e.g., Kennett & Shackleton, 1976; Miller et al., 1991; Zachos et al., 1996) but the stratigraphy of events and the extent of cooling relative to ice growth across the EOT is controversial (e.g., Bohaty et al., 2012; Coxall et al., 2005; Coxall & Wilson, 2011; Katz et al., 2008; Kennett & Shackleton, 1976; Wade et al., 2012). Benthic oxygen isotope ($\delta^{18}O$) values increase in two steps across the EOT in the best resolved deep ocean records (Bohaty et al., 2012; Coxall et al., 2005). Step 1, the first of these shifts, was smaller and occurred ~300 kyr prior to Step 2, which represents the major climatic shift close to the base of geomagnetic polarity chron C13n. Oxygen isotope records in benthic foraminifera are often well preserved in Ocean Drilling Program (ODP) cores (Edgar et al., 2013). However, $\delta^{18}O$ records in planktic foraminiferal calcite from carbonate-rich settings are more susceptible to diagenetic alteration (Sexton et al., 2006, and references therein). Thus, reliable geochemical records from shallow shelf and deep-sea upper water column environments are rare (Wilson & Opdyke, 1996). Geochemical analysis of foraminifera derived from clay-rich lithologies offers a way to resolve this lack of data because of the unusually high preservation potential of calcareous microfossils in these low porosity and low permeability sediments (e.g., Norris & Wilson, 1998; Pearson et al., 2001; Wilson & Norris, 2001). High-resolution upper water column foraminiferal stable isotope and Mg/Ca records have been obtained across the EOT from ODP sites in the Southern Ocean and South Atlantic Ocean, and from marginal-marine sediments from the Gulf Coast, USA, and Tanzania (Bohaty et al., 2012; Katz et al., 2008; Lear et al., 2008; Peck et al., 2010; Wade et al., 2012); however, detailed information from shallow water paleoclimate settings is rare across the EOT, especially from middle- to high-latitude sites (Liu et al., 2009, 2018).
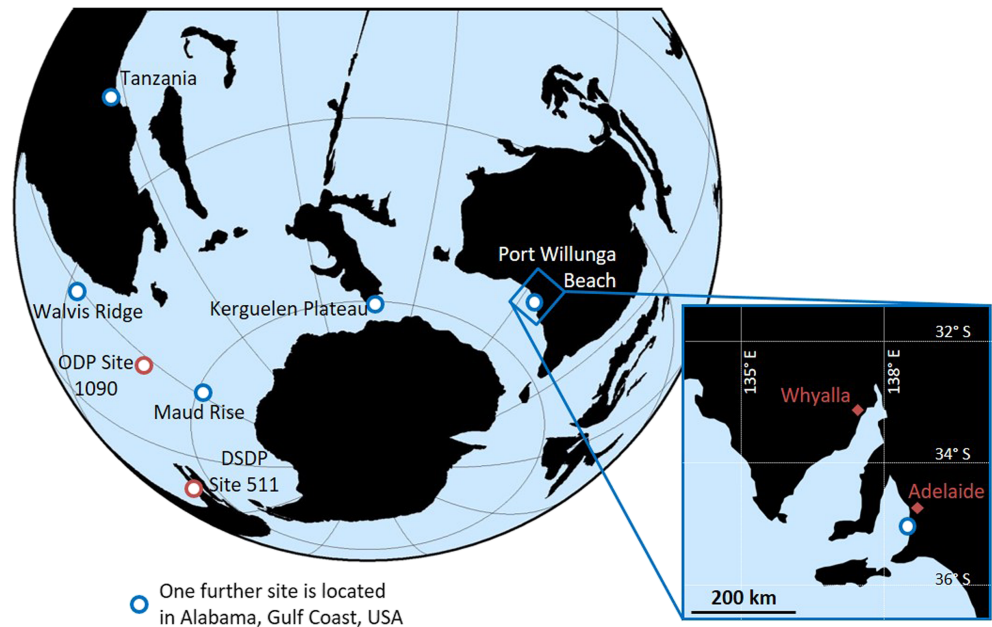
Figure 1. Tectonic reconstruction of Antarctica and its surrounding continents at 34 Ma (obtained from the Ocean Drilling Stratigraphic Network, after Hay et al., 1999) also showing study sites for published stable isotope and Mg/Ca records that span Step 1 of the EOT (blue open circles; see text for details) (Bohaty et al., 2012; Katz et al., 2008; Lear et al., 2008; Peck et al., 2010; Wade et al., 2012). Also shown are sites where latest Eocene alkenone-based sea surface temperature records have been collected (red open circles; see text for details) (Liu et al., 2009; Liu et al., 2018; Plancq et al., 2014). Inset: study site location in South Australia in present geographic coordinates.

Here we address this knowledge gap from one of the numerous shallow marine basins that was active along the southern Australian margin during the Eocene and Oligocene (McGowran et al., 2004), by studying a shallow shelf sedimentary sequence from Port Willunga Beach, South Australia (51°S paleolatitude) (Figure 1). We report new magnetostratigraphic and chemostratigraphic data sets and integrate these records with published biostratigraphic controls (McGowran, 1987; McGowran, 2009; McGowran et al., 2004; McGowran et al., 2016; McGowran & Beecroft, 1986a, 1986b). To assess paleoenvironmental change, we present $\delta^{18}O$ and $\delta^{13}C$ records from analysis of whole benthic foraminifera specimens, and Mg/Ca data obtained by laser ablation inductively coupled mass spectrometer (LA-ICPMS) analysis of the same fauna.

In this work, we report a high-resolution record of EOT climatic change from clay-rich sediments at Port Willunga Beach. Our results identify, for the first time, the stratigraphic position of the EOT at Port Willunga Beach and the temperature change across Step 1, which provides the first high-resolution shallow water environmental record across EOT Step 1 for a paleolatitude between 35° and 57° from the Southern Hemisphere.

2. Study Site and Methods

The cliffs behind Port Willunga Beach consist of shallow shelf and terrestrial Eocene-Oligocene sediments that are overlain unconformably by Quaternary marine muds. The portion of the Late Eocene Blanche Point Formation (BPF) investigated for this study is a clay-rich, biosiliceous mudstone that contains well-preserved benthic foraminifera (McGowran et al., 2004). The sequence was deposited in a coastal embayment in water depths of <100 m based on ostracod assemblages and considering the spatial and stratigraphic distribution of sediments throughout the Saint Vincent Basin (James & Bone, 2000). There is no stratigraphic or biostratigraphic evidence of significant water depth changes through this portion of the BPF (James & Bone, 2000; McGowran et al., 2004; McGowran & Beecroft, 1986a). An unconformity occurs above the BPF, and early Oligocene erosion has removed up to 50 m of the upper BPF in some areas (McGowran et al., 2004). We studied the Port Willunga Beach section where erosion of the BPF is minimized (McGowran et al., 2016). Above the unconformity lie terrestrial deposits of the Chinaman Gully

Formation (CGF). This unit contains a succession of carbonaceous sands, clays, soils, and littoral sands that grade into the shallow marine, transgressive Port Willunga Formation (PWF) (McGowran et al., 2004). Benthic and planktonic foraminiferal biostratigraphy confirms that the PWF was deposited in the earliest Oligocene (McGowran et al., 2004) at shallower water depths than the BPF (James & Bone, 2000; McGowran et al., 2004). Prior to this study, the stratigraphic position of the EOT at Port Willunga Beach was uncertain (McGowran, 1987; McGowran & Beecroft, 1986a, 1986b) because of the lack of a well-developed magnetostratigraphy and oxygen isotope stratigraphy, which we address here.

We collected samples from a cliff section at Port Willunga (latitude −35.250°S, longitude 138.462°E). The location and stratigraphic position of all sampled horizons, and paleomagnetic methods and results are presented in the supporting information. Foraminifera tests are "near glassy" in appearance (cf. Sexton et al., 2006) in most sampled horizons in the BPF. *Cibicides* cf. *perforatus* specimens are common in all samples that contain foraminifera. Foraminifera tests from the PWF have a frosted appearance (cf. Sexton et al., 2006) with enlarged pores and were not used for geochemical analysis.

We selected whole *C*. cf. *perforatus* specimens, 200 to 300 μm in diameter, for geochemical analysis. Only tests that were free of diagenetic calcite crystals visible on test surfaces at 4X magnification under a light microscope were selected. Nine to 12 *C*. cf. *perforatus* tests (200 ± 20 μg) were analyzed from each sampled horizon for $\delta^{18}O$ and $\delta^{13}C$ using a Finnigan MAT 251 mass spectrometer. Sample preparation methods, stable isotopic analytical methods, and corrected $\delta^{18}O$ and $\delta^{13}C$ data are presented in the supporting information. LA-ICPMS Mg/Ca analysis was performed (cf. Creech et al., 2010; Sadekov et al., 2008; Sadekov et al., 2009) to ensure that Mg/Ca results reflect a primary, biogenic signal for *C*. cf. *perforatus* tests. Mg/Ca analytical methods and data are presented in the supporting information.

3. Results and Discussion

3.1. Microfossil Taphonomy

Roughly 5% of foraminifera tests in the sediment have a "glassy" appearance (cf. Sexton et al., 2006), and the taphonomy of most of the remainder can be described as near-glassy to moderately frosty in the relatively clay-rich BPF (an example of a near-glassy specimen is shown in the supporting information). Several specimens of *C*. cf. *perforatus* from the BPF were broken open and inspected: no diagenetic calcite crystals or foreign material was visible. Foraminifera are absent from a 2-m-thick zone in the upper BPF. It is unclear whether this absence results from foraminifera test dissolution or an environmental control.

"Glassy" and "near-glassy" specimens were selected for geochemical analysis. Trace element LA-ICPMS profiling reveals that all analyzed *C*. cf. *perforatus* tests have cyclic compositional banding in Mg/Ca through test chamber walls where Al/Ca is <0.15 mmol/mol (Figure 2; supporting information), which indicates that diagenetic alteration has not affected calcite composition (Eggins et al., 2004; Erez, 2003). Low Al/Ca indicates that Mg-rich clays and terrestrial inorganic calcite precipitation have not affected inner parts of test chamber walls (Creech et al., 2010). Thus, LA-ICPMS profiles allowed selection of data from within test chamber walls that are likely to have recorded paleoclimatic conditions.

3.2. Stratigraphy

Waghorn (1989) identified the highest occurrence of the calcareous nannofossil *Discoaster saipanensis* (NP19/20-NP21 boundary) in the Gull Rock Member of the BPF, ~12.5 m below the unconformity between the BPF and the CGF (Figure 3). No other first or last appearance datums have been identified in the portion of the stratigraphic section that we sampled at Port Willunga. Biostratigraphic results from McGowran et al. (2004) and McGowran (2009) indicate that the base of the PWF was deposited during C13n. Our paleomagnetic results indicate that BPF sediments record reversed polarities, while normal polarity is recorded in both the CGF and the lower PWF (Figure 3; supporting information). Thus, the BPF is ascribed to polarity chron C13r, which includes nannofossil zone NP19/20-NP21 (Agnini et al., 2014); both the C13r/C13n reversal boundary and the Eocene-Oligocene (E-O) boundary fall within the unconformity with the overlying CGF. We do not have paleomagnetic results from within 0.5 m of the BPF-CGF boundary; however, we infer that the C13r/C13n reversal boundary coincides with this lithological change.

Our stable isotopic data indicate little variability throughout the lowermost 6 m of the BPF (Figure 3). Above the zone where foraminifera are absent from the sediment, there is a clear $\delta^{18}O$ increase and a significant
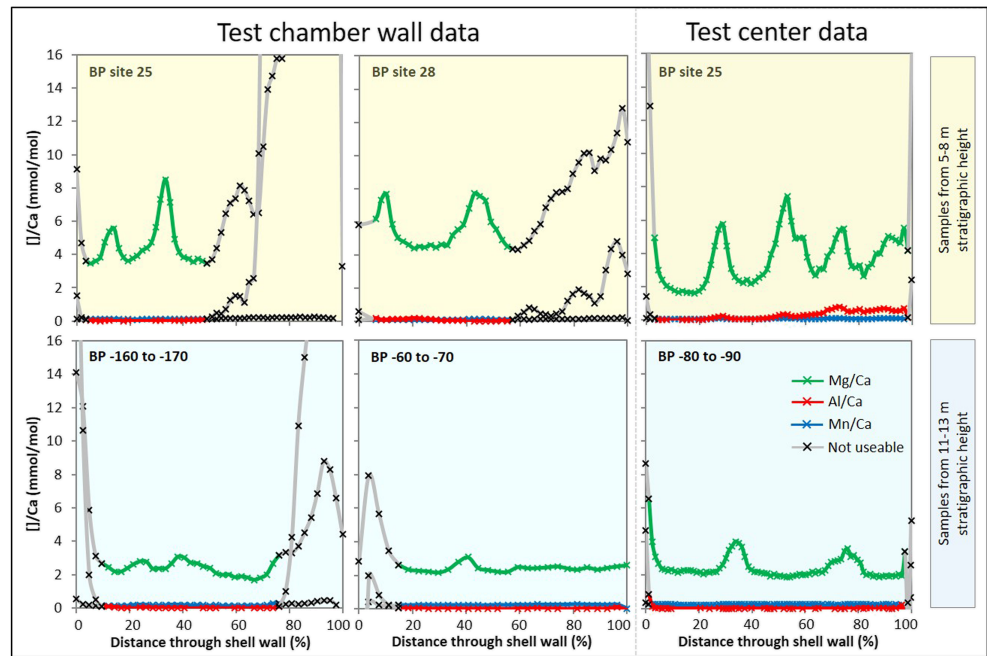
Figure 2. Examples of cyclic compositional banding through foraminifera test chamber walls and test centers. Yellow shading represents data from before EOT Step 1; blue shading represents data from between Steps 1 and 2. Data are deemed unusable where Al/Ca >0.15 mmol/mol.
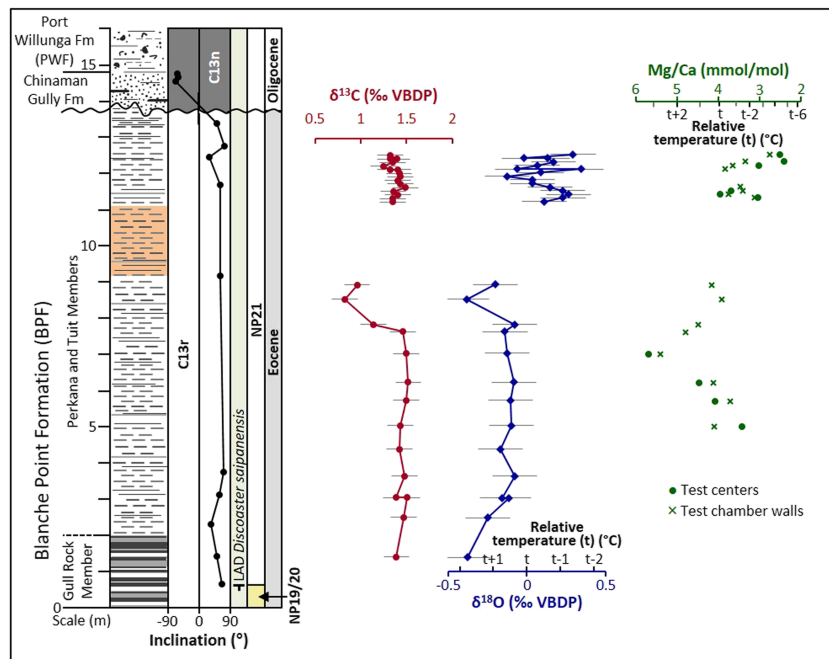

Figure 3. Stable isotopic and Mg/Ca data for the Late Eocene Blanche Point Formation, South Australia. The stratigraphy of the studied section is indicated. Paleomagnetic data and the C13r-C13n boundary are shown. $\delta^{18}O$ (blue diamonds) and $\delta^{13}C$ (red solid circles) data are shown with 95% confidence intervals. The relative temperature scale shown for the $\delta^{18}O$ data is calculated using the *Cibicidoides* $\delta^{18}O$-*T* relationship of Lynch-Stieglitz et al. (1999). Green crosses represent LA-ICPMS Mg/Ca data for profiles through the umbilical side of test chamber walls and green solid circles represent data from the umbilical side of test centers. The relative temperature scale shown for Mg/Ca data was calculated using equation (2) and an *A* value of 0.109 (Lear et al., 2002; Martin et al., 2002). The interval that lacks *Cibicides* cf. *perforatus* specimens is shaded orange between 9.2 and 11.1 m.

Mg/Ca decrease relative to below this zone. A transient Mg/Ca increase that records a possible pre-EOT warming event is apparent at ~7-m stratigraphic height. A similar Mg/Ca signal is apparent in the high-resolution record of Lear et al. (2008) from Tanzania, but it is not apparent in other Mg/Ca records that have sufficient data density to resolve this event (Bohaty et al., 2012; Peck et al., 2010). This observation suggests that the Mg/Ca increase is not a global signal but rather a local or possibly regional event.

A pronounced, negative $\delta^{13}C$ excursion occurs immediately below the zone where *C*. cf. *perforatus* is absent. Above this zone, $\delta^{13}C$ returns to pre-excursion values (Figure 3). This $\delta^{13}C$ structure is correlative to records from Maud Rise (ODP Site 689; Diester-Haass & Zahn, 1996) and Walvis Ridge (ODP Site 522; Zachos et al., 1996), where it occurs roughly two thirds of the way through C13r, immediately before EOT Step 1. This $\delta^{13}C$ structure is also evident in data from Tanzania (Pearson et al., 2008), the equatorial Pacific Ocean (ODP Site 1218; Coxall et al., 2005; Coxall & Wilson, 2011), and the South Atlantic Ocean (ODP Sites 1090 and 1265; Pusz et al., 2011), which suggests that it is a global stratigraphic feature. Katz et al. (2008), supporting information) also inferred this $\delta^{13}C$ structure at Saint Stephen′s Quarry, Alabama, and suggested that it is correlative with the Walvis Ridge and equatorial Pacific records. The idea that this is a global event immediately preceding EOT Step 1 is discussed by Coxall et al. (2018). The fact that this negative $\delta^{13}C$ structure is recorded at Port Willunga Beach (together with paleomagnetic and biostratigraphic attribution of these sediments to C13r) indicates that the lowermost ~10 m of the studied stratigraphic section records the interval immediately preceding EOT Step 1.

We infer that most of EOT Step 1 occurred in the zone in which *C*. cf. *perforatus* is absent because: (1) The portion of the record above this zone has distinct $\delta^{18}O$ and Mg/Ca results from those below this zone, (2) the portion of the record above this zone does not have $\delta^{18}O$ and Mg/Ca trends (as would be expected within Step 1 or 2), and (3) because the $\delta^{18}O$ plateau following EOT Step 2 occurs during C13n, whereas this portion of our record falls within C13r. Also, the magnitude of $\delta^{18}O$ change across this zone is insufficient to have recorded EOT Step 2; global results consistently indicate an ~1‰ to 1.5‰ $\delta^{18}O$ shift across EOT Steps 1 and 2 combined (e.g., Bohaty et al., 2012; Coxall et al., 2005; Katz et al., 2008; Lear et al., 2008; Peck et al., 2010; Pusz et al., 2011; Wade et al., 2012), which is not seen here (Figure 3). Therefore, the portion of the record above the zone where *C*. cf. *perforates* is absent represents the time interval following Step 1, which is referred to as the $\delta^{18}O$ plateau between Steps 1 and 2 in the stratigraphy of Coxall et al. (2005). The upper part of Chron C13n is recorded just above the unconformity with the overlying CGF; thus, sediments deposited during approximately half of Chron C13n, including during EOT Step 2, are inferred to have been removed by earliest Oligocene subaerial erosion at Port Willunga Beach. A minimum mean sedimentation rate of 1.8 cm/kyr is estimated for the upper BPF by interpolating between the highest occurrence of *D. saipanensis* (34.44 Ma; Blaj et al., 2009) and the beginning of Step 2 (~33.7 Ma; Bohaty et al., 2012). This sedimentary section, therefore, affords an opportunity to assess environmental change across this time interval.

Our stratigraphy is consistent with a lithological interpretation of sea level change at the study site. Relative sea level fall must have occurred prior to deposition of the CGF. This is consistent with accelerated EOT cooling and Antarctic ice sheet growth associated with EOT Step 2.

3.3. Paleotemperature

The $\delta^{18}O$ in *C*. cf. *perforatus* shifts from an average of −0.1‰ to 0.3‰ VPDB across EOT Step 1. We estimate absolute seawater temperature assuming (i) negligible continental ice volume immediately prior to Step 1 (e.g., Shackleton & Kennett, 1975), (ii) no local salinity change, and (iii) a local seawater $\delta^{18}O$ value equal to the estimated global mean values of −1.27‰ and −1.1‰ VSMOW for an ice-free world (after Shackleton and Kennett (1975) and Bohaty et al. (2012), respectively). Note that the seawater $\delta^{18}O$ value from Shackleton and Kennett (1975) is corrected to −1.27‰ VSMOW to account for the modern conversion factor between VPDB and VSMOW (Hut, 1987). Note also that seawater $\delta^{18}O$ varies with latitude in the modern surface ocean, which reflects the imprint of the hydrological cycle; however, at 51°S modern surface seawater $\delta^{18}O$ is not significantly different to the global mean value (Zachos et al., 1994). We calculate surface seawater temperature change using the linear *Cibicidoides*-based equations of Lynch-Stieglitz et al. (1999) and Marchitto et al. (2014), which both take the form of equation (1):

$$\delta^{18}O_{Cib} \text{ (VPDB)} = \left[\delta^{18}O_{water} \text{ (VSMOW)} - 0.27\right] - aT + b, \tag{1}$$

where T is temperature and a and b have values of 0.21 and 3.38 or 0.224 and 3.53 in Lynch-Stieglitz et al. (1999) and Marchitto et al. (2014), respectively. Using the two seawater $\delta^{18}O$ values given above and the two linear $\delta^{18}O$-temperature relationships referenced, we calculate a fall in surface seawater temperature from about 10 °C to 8 °C or from 9 °C to 7 °C across EOT Step 1. The same result is found using the quadratic *Cibicidoides*-based $\delta^{18}O$-temperature relationship of Marchitto et al. (2014).

We next compare $\delta^{18}O$-derived temperatures with our Mg/Ca data. Mg/Ca is typically higher below Step 1 (average Mg/Ca = 4.33 mmol/mol in foraminiferal test chamber walls) than above it (average Mg/Ca = 3.42 mmol/mol in foraminiferal test chamber walls). This pre-Step 1 average includes all data below Step 1; removing the outlying data point at ~7-m stratigraphic height from our calculation does not affect significantly our conclusions. Lear et al. (2008) presented the only published high-resolution EOT Mg/Ca record for a shelf environment using *Cibicidoides*. They employed the exponential relationship of Lear et al. (2002) between foraminiferal Mg/Ca and seawater temperature, as given in equation (2):

$$Mg/Ca_{Cib} = Xe^{AT}, \tag{2}$$

where T is seawater temperature and A and X are empirical constants. Both Martin et al. (2002) and Lear et al. (2002) found that $A = 0.109$ for *Cibicidoides* spp. We use this A value to be consistent with Lear et al. (2008), and because the Mg/Ca-T relationship of Lear et al. (2002) has been applied previously to LA-ICPMS Mg/Ca data for Eocene *Cibicidoides* spp. (Creech et al., 2010). This equation also yields an ~2 °C cooling across Step 1, which is consistent with our $\delta^{18}O$ data, and indicates that the stable isotopic shift across Step 1 can be attributed wholly to temperature change. This result does not preclude the possibility of Antarctic ice immediately prior to the EOT (e.g., Zachos et al., 1999), but it suggests that, at this site, there is no evidence for a major ice volume increase during Step 1 despite the documented cooling. Uncertainty associated with our *C. cf. perforates* $\delta^{18}O$ values (± 0.14‰; supporting information) means that a further 0.14‰ shift may have occurred across Step 1 that is not accounted for in our Mg/Ca-temperature results. Thus, our results are consistent with evidence for comparatively minor ice growth across Step 1 (e.g., Katz et al., 2008; Pusz et al., 2011).

To assess the validity of our $\delta^{18}O$-derived absolute temperature estimates, we calculate independent latest Eocene seawater $\delta^{18}O$ using a literature estimate of latest Eocene seawater Mg/Ca (2.5 mmol/mol; from Evans and Müller (2012)), then compare the results with the latest Eocene seawater $\delta^{18}O$ value used above (cf. Burgess et al., 2008). Literature values for seawater Mg/Ca can be related to X values in Equation (2) by assuming that the relationship between foraminiferal calcite composition and seawater chemistry is purely abiotic (equation (3)).

$$X = \frac{Mg/Ca_{SW}^{t_t}}{Mg/Ca_{SW}^{t_0}} B, \tag{3}$$

where X is as in equation (2), t_0 is the present time, t_t is a time in the past, and B is a species-specific, empirically derived constant, which is equivalent to X when $t_0 = t_t$. Lear et al. (2002) and Martin et al. (2002) obtained B values for modern *Cibicidoides* spp. of 0.867 mmol/mol and 1.22 mmol/mol, respectively. X values of 0.43 and 0.61, respectively, are obtained assuming that modern seawater Mg/Ca is 5.2 mmol/mol, and latest Eocene seawater Mg/Ca is 2.5 mmol/mol (Evans & Müller, 2012). These X values give latest Eocene surface seawater temperatures of 21 °C or 18 °C (from equation (2), using an A value of 0.109 after Martin et al. (2002) and Lear et al. (2002) and our pre-Step 1 foraminiferal Mg/Ca value of 4.33 mmol/mol). These temperature estimates are consistent with latest Eocene alkenone-based surface ocean temperatures calculated for Southern Ocean sites at similar paleolatitudes to our study site (Deep-Sea Drilling Project Site 511 and ODP Site 1090; Liu et al., 2009; Plancq et al., 2014; Liu et al., 2018).

Latest Eocene surface seawater $\delta^{18}O$ would have been between 0.57‰ and 1.34‰ VSMOW using all combinations of the above Mg/Ca-temperature results, our pre-Step 1 foraminiferal $\delta^{18}O$ value, and the equations of Lynch-Stieglitz et al. (1999) and Marchitto et al. (2014). These values are significantly greater than accepted values for an ice-free world. This discrepancy cannot be explained by ice growth, which would
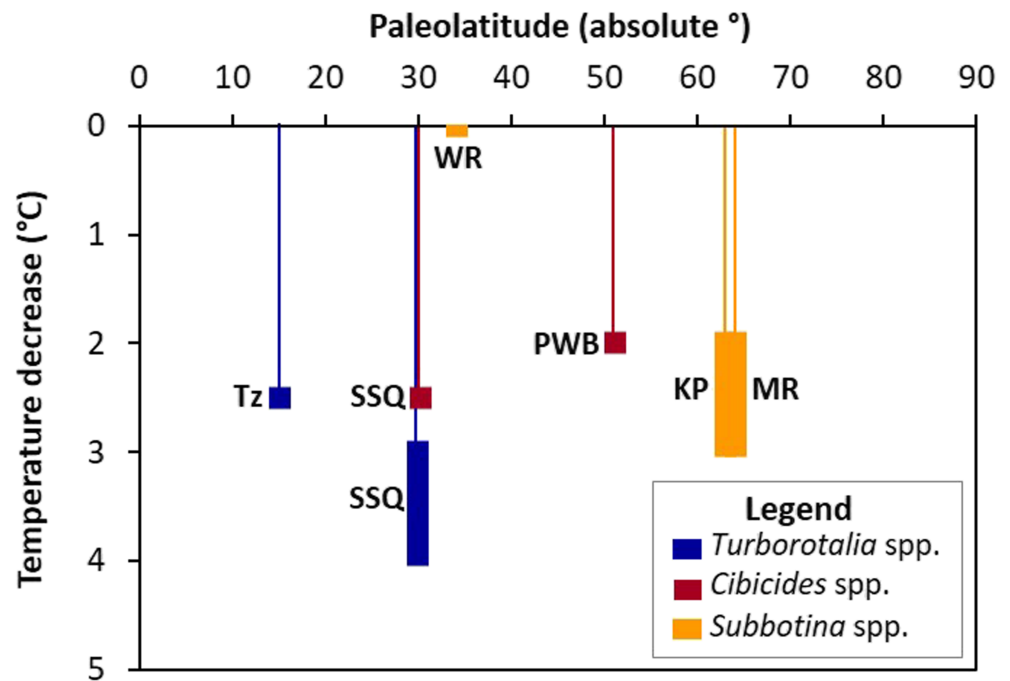
Figure 4. Estimated temperature decrease across Step 1 of the EOT with paleolatitude for all high-resolution Mg/Ca-temperature records across the interval. Estimated temperature range values (solid color bars) are from literature sources. Colors indicate foraminifera genera, as indicated in the legend. Locations are Maud Rise (MR) (64°S), *S. angioporides* (Bohaty et al., 2012); Kerguelen Plateau (KP) (63°S), *S. angiporoides* (Bohaty et al., 2012); Port Willunga Beach (PWB) (51° S), *C.* cf. *perforatus* (this study); Walvis Ridge (WR) (34°S), *S. utilizindex* (Peck et al., 2010); Tanzania (Tz) (15°S), *T. ampliapertura* (Lear et al., 2008); Saint Stephen's Quarry, Alabama (SSQ) (30°N), *C. pippeni* and *C. Cocoaensis* (Katz et al., 2008); SSQ, Alabama (30°N), *T. ampliapertura* (Wade et al., 2012).

decrease surface seawater δ^{18}O. It cannot be explained by sensitivity to error in our foraminiferal Mg/Ca results: a one standard deviation (0.55 mmol/mol) change from our average measured pre-Step 1 foraminiferal Mg/Ca value results in a surface seawater δ^{18}O change of less than $\pm$0.27‰ using the *B* values of both Lear et al. (2002) and Martin et al. (2002). The discrepancy cannot be explained by partial dissolution of our sample material; dissolution would decrease foraminiferal Mg/Ca (e.g., Rongstad et al., 2017), which would lead to lower seawater temperatures, and, thus, lower calculated values for latest Eocene surface seawater δ^{18}O. Areas where recrystallization or clay contamination has occurred can be recognized and removed from LA-ICPMS Mg/Ca data (see supporting information). Thus, we conclude that seawater δ^{18}O in this embayment was closer to +1 than to −1 in the latest Eocene, regardless of the *Cibicidoides* δ^{18}O-temperature relationship or the literature value employed for surface seawater δ^{18}O in an ice-free world.

Higher surface seawater δ^{18}O values can explain the discrepancy between published estimates for midlatitude seawater δ^{18}O in an ice-free world, our data, and literature values for latest Eocene seawater Mg/Ca. Higher surface seawater δ^{18}O could result from local evaporation within the embayment where the sediments were deposited; however, it is unlikely that net evaporative conditions existed at the paleolatitude of our study site. McGowran et al. (1997) documented fossil faunal assemblages along the southern Australian margin from the late-Middle Eocene onward that are characteristic of higher seawater temperatures than would be expected for the site paleolatitude at the time of deposition. They attributed this finding to development of a proto-Leeuwin Current, which may have transported relatively saline surface waters from evaporative subtropical areas to the southern Australian coastline. The surface ocean evaporative zone may have also expanded to higher latitudes globally in the relatively warm latest Eocene. Petersen and Schrag (2015) calculated a thermocline seawater δ^{18}O value of +1.27‰ VSMOW for the latest Eocene at Maud Rise using clumped isotope paleothermometry and foraminiferal δ^{18}O, which is similar to our

result. Further work is needed to ascertain if relatively high surface seawater $\delta^{18}O$ was widespread in the Southern Hemisphere midlatitudes during the latest Eocene.

3.4. Comparisons With Global Shallow Water, High-Resolution Mg/Ca Records Across Step 1

High-resolution, shallow shelf and deep-sea upper water column Mg/Ca records across Step 1 exist for planktic foraminifera from Maud Rise, Kerguelen Plateau, Walvis Ridge, Tanzania, and Saint Stephen's Quarry, Alabama (Bohaty et al., 2012; Lear et al., 2008; Peck et al., 2010; Wade et al., 2012), and for benthic foraminifera from Saint Stephen's Quarry, where paleowater depths were ~100–115 m (Katz et al., 2008) (Figure 1). These records are compiled along with our data in Figure 4. At all sites, Mg/Ca values were higher before Step 1 than between Steps 1 and 2, which suggests that cooling across Step 1 was global. Our calculated temperature change across Step 1 is similar to most literature values (Figure 4). Our data from 51°S, therefore, lend support to the suggestion that the amplitude of cooling did not increase with latitude. This, in turn, suggests that cryospheric changes associated with cooling across EOT Step 1 were modest, and it contradicts the mechanism suggested to explain the northward migration of the EOT intertropical convergence zone in the equatorial Pacific Ocean inferred from dust geochemistry (Hyeong et al., 2016).

4. Conclusions

We present the first shallow water, high-resolution stable isotopic and trace element record of Step 1 of the EOT for a paleolatitude between 35° and 57° from either hemisphere, using well-preserved tests of the benthic foraminiferid *C*. cf. *perforatus* collected from Port Willunga Beach, South Australia. This is the first high-resolution $\delta^{13}C$, $\delta^{18}O$, and Mg/Ca record of paleoclimatic change across this interval obtained from terrestrially exposed sediments. A pronounced, negative $\delta^{13}C$ excursion occurred immediately before Step 1, which is likely a globally correlative event. Results are interpreted to indicate an ~2 °C cooling and negligible ice volume change across EOT Step 1. When compared to published data sets from around the world we infer that there was no polar amplification of the cooling signal across Step 1. This result supports the interpretation that ice volume change was negligible and contradicts the mechanism suggested to explain the inferred northward migration of the intertropical convergence zone in the equatorial Pacific Ocean during the EOT. Our geochemical data are interpreted to indicate that surface seawater $\delta^{18}O$ was higher than is typical for the study site latitude. This may have been due to local evaporation, transportation of relatively saline surface waters from evaporative subtropical areas by the proto-Leeuwin current, or a surface ocean evaporative zone expansion to higher latitudes globally in the relatively warm latest Eocene. Further data are needed to identify the source of this saline water. Terrestrially exposed, clay-rich Paleogene marginal-marine sediments of the type studied here represent a promising archive for future paleoclimatic studies.

References

Agnini, C., Fornaciari, E., Raffi, I., Catanzariti, R., Pälike, H., Backman, J., & Rio, D. (2014). Biozonation and biochronology of Paleogene calcareous nannofossils from low and middle latitudes. *Newsletters on Stratigraphy*, *47*(2), 131–181.

Blaj, T., Backman, J., & Raffi, I. (2009). Late Eocene to Oligocene preservation history and biochronology of calcareous nannofossils from paleo-equatorial Pacific Ocean sediments. *Rivista Italiana di Paleontologia e Stratigrafia*, *115*, 67–85.

Bohaty, S. M., Zachos, J. C., & Delaney, M. L. (2012). Foraminiferal Mg/Ca evidence for Southern Ocean cooling across the Eocene-Oligocene transition. *Earth and Planetary Science Letters*, *317*, 251–261.

Burgess, C. E., Pearson, P. N., Lear, C. H., Morgans, H. E., Handley, L., Pancost, R. D., & Schouten, S. (2008). Middle Eocene climate cyclicity in the southern Pacific: Implications for global ice volume. *Geology*, *36*, 651–654.

Coxall, H. K., Huck, C. E., Huber, M., Lear, C. H., Legarda-Lisarri, A., O'Regan, M., et al. (2018). Export of nutrient rich Northern Component Water preceded early Oligocene Antarctic glaciation. *Nature Geoscience*, *11*(3), 190–196. https://doi.org/10.1038/s41561-018-0069-9

Coxall, H. K., & Wilson, P. A. (2011). Early Oligocene glaciation and productivity in the eastern equatorial Pacific: Insights into global carbon cycling. *Paleoceanography*, *26*, PA2221. https://doi.org/10.1029/2010PA002021

Coxall, H. K., Wilson, P. A., Palike, H., Lear, C. H., & Backman, J. (2005). Rapid stepwise onset of Antarctic glaciation and deeper calcite compensation in the Pacific Ocean. *Nature*, *433*, 53–57.

Creech, J. B., Baker, J. A., Hollis, C. J., Morgans, H. E., & Smith, E. G. (2010). Eocene sea temperatures for the mid-latitude southwest Pacific from Mg/Ca ratios in planktonic and benthic foraminifera. *Earth and Planetary Science Letters*, *299*, 483–495.

Diester-Haass, L., & Zahn, R. (1996). Eocene-Oligocene transition in the Southern Ocean: History of water mass circulation and biological productivity. *Geology*, *24*, 163–166.

Edgar, K. M., Pälike, H., & Wilson, P. A. (2013). Testing the impact of diagenesis on the $\delta^{18}O$ and $\delta^{13}C$ of benthic foraminiferal calcite from a sediment burial depth transect in the equatorial Pacific. *Paleoceanography*, *28*, 468–480. https://doi.org/10.1002/palo.20045

Eggins, S. M., Sadekov, A., & De Deckker, P. (2004). Modulation and daily banding of Mg/Ca in Orbulina universa tests by symbiont photosynthesis and respiration: A complication for seawater thermometry? *Earth and Planetary Science Letters*, *225*, 411–419.

Erez, J. (2003). The source of ions for biomineralization in foraminifera and their implications for paleoceanographic proxies. *Reviews in Mineralogy and Geochemistry*, *54*, 115–149.

Evans, D., & Müller, W. (2012). Deep time foraminifera Mg/Ca paleothermometry: Nonlinear correction for secular change in seawater Mg/Ca. *Paleoceanography*, *27*, PA4205. https://doi.org/10.1029/2012PA002315

Hay, W., DeConto, R., Wold, C., Wilson, K., Voigt, V., Schulz, M., et al. (1999). Alternative global Cretaceous paleogeography. In E. Barrera, & C. Johnson (Eds.), *The evolution of Cretaceous ocean/climate systems, Geological Society of America Special Paper 332*, *Geological Society of America* (pp. 1–47). Boulder, CO: The Geological Society of America, Inc.

Hut, G. (1987). Consultants' group meeting on stable isotope reference samples for geochemical and hydrological investigations, *Rep. to Dir. Gen., Int. Atomic Energy Agency, Vienna, 1-42.*

Hyeong, K., Kuroda, J., Seo, I., & Wilson, P. A. (2016). Response of the Pacific inter-tropical convergence zone to global cooling and initiation of Antarctic glaciation across the Eocene Oligocene Transition. *Scientific Reports*, *6*, 30647.

James, N. P., & Bone, Y. (2000). Eocene cool-water carbonate and biosiliceous sedimentation dynamics, St Vincent Basin, South Australia. *Sedimentology*, *47*, 761–786.

Katz, M. E., Miller, K. G., Wright, J. D., Wade, B. S., Browning, J. V., Cramer, B. S., & Rosenthal, Y. (2008). Stepwise transition from the Eocene Greenhouse to the Oligocene Icehouse. *Nature Geoscience*, *1*, 329–334.

Kennett, J. P., & Shackleton, N. J. (1976). Oxygen isotopic evidence for the development of the psychrosphere 38 Myr ago. *Nature*, *260*, 513–515.

Lear, C. H., Bailey, T. R., Pearson, P. N., Coxall, H. K., & Rosenthal, Y. (2008). Cooling and ice growth across the Eocene-Oligocene transition. *Geology*, *36*, 251–254.

Lear, C. H., Rosenthal, Y., & Slowey, N. (2002). Benthic foraminiferal Mg/Ca-paleothermometry: A revised core-top calibration. *Geochimica et Cosmochimica Acta*, *66*, 3375–3387.

Liu, Z., He, Y., Jiang, Y., Wang, H., Liu, W., Bohaty, S. M., & Wilson, P. A. (2018). Transient temperature asymmetry between hemispheres in the Palaeogene Atlantic Ocean. *Nature Geoscience*, *11*(9), 656.

Liu, Z., Pagani, M., Zinniker, D., DeConto, R., Huber, M., Brinkhuis, H., et al. (2009). Global cooling during the Eocene-Oligocene climate transition. *Science*, *323*(5918), 1187–1190. https://doi.org/10.1126/science.1166368

Lynch-Stieglitz, J., Curry, W. B., & Slowey, N. (1999). A geostrophic transport estimate for the Florida Current from the oxygen isotope composition of benthic foraminifera. *Paleoceanography*, *14*, 360–373.

Marchitto, T. M., Curry, W. B., Lynch-Stieglitz, J., Bryan, S. P., Cobb, K. M., & Lund, D. C. (2014). Improved oxygen isotope temperature calibrations for cosmopolitan benthic foraminifera. *Geochimica et Cosmochimica Acta*, *130*, 1–11.

Martin, P. A., Lea, D. W., Rosenthal, Y., Shackleton, N. J., Sarnthein, M., & Papenfuss, T. (2002). Quaternary deep sea temperature histories derived from benthic foraminiferal Mg/Ca. *Earth and Planetary Science Letters*, *198*, 193–209.

McGowran, B. (1987). Late Eocene perturbations: Foraminiferal biofacies and evolutionary overturn, southern Australia. *Paleoceanography*, *2*, 715–727.

McGowran, B. (2009). The Australo-Antarctic Gulf and the Auversian Facies Shift. In C. Koeberl & A. Montanari (Eds.), *The Late Eocene Earth—Hothouse, Icehouse, and Impacts*, *Geological Society of America Special Paper 452, Ch* (Vol. 14, pp. 215–240). Boulder, CO: The Geological Society of America, Inc. https://doi.org/10.1130/2009.2452(14)

McGowran, B., & Beecroft, A. (1986a). Foraminiferal biofacies in a silica-rich neritic sediment, Late Eocene, South-Australia. *Palaeogeography Palaeoclimatology Palaeoecology*, *52*, 321–345.

McGowran, B., & Beecroft, A. (1986b). Neritic, southern extratropical foraminifera and the terminal Eocene event. *Palaeogeography Palaeoclimatology Palaeoecology*, *55*, 23–34.

McGowran, B., Holdgate, G. R., Li, Q., & Gallagher, S. J. (2004). Cenozoic stratigraphic succession in southeastern Australia. *Australian Journal of Earth Sciences*, *51*, 459–496.

McGowran, B., Lemon, N., Preiss, W., & Olliver, J. (2016). Geological field excursion guide—Cenozoic Willunga Embayment: From Australo-Antarctic Gulf to Sprigg Orogeny. Report Book 2016/00008, Department of State Development, South Australia, and Geological Society of Australia*, South Australian Division, 48 p.

McGowran, B., Li, Q., Cann, J., Padley, D., McKirdy, D. M., & Shafik, S. (1997). Biogeographic impact of the Leeuwin Current in southern Australia since the late middle Eocene. *Palaeogeography Palaeoclimatology Palaeoecology*, *136*, 19–40.

Miller, K. G., Wright, J. D., & Fairbanks, R. G. (1991). Unlocking the ice house: Oligocene-Miocene oxygen isotopes, eustasy, and margin erosion. *Journal of Geophysical Research*, *96*(B4), 6829–6848.

Norris, R. D., & Wilson, P. A. (1998). Low-latitude sea-surface temperatures for the mid-Cretaceous and the evolution of planktic foraminifera. *Geology*, *26*, 823–826.

Pearson, P. N., Ditchfield, P. W., Singano, J., Harcourt-Brown, K. G., Nicholas, C. J., Olsson, R. K., et al. (2001). Warm tropical sea surface temperatures in the Late Cretaceous and Eocene epochs. *Nature*, *413*(6855), 481–487. https://doi.org/10.1038/35097000

Pearson, P. N., McMillan, I. K., Wade, B. S., Dunkley Jones, T., Coxall, H. K., Bown, P. R., & Lear, C. H. (2008). Extinction and environmental change across the Eocene-Oligocene boundary in Tanzania. *Geology*, *36*, 179–182.

Peck, V. L., Yu, J., Kender, S., & Riesselman, C. R. (2010). Shifting ocean carbonate chemistry during the Eocene-Oligocene climate transition: Implications for deep-ocean Mg/Ca paleothermometry. *Paleoceanography*, *25*, PA4219. https://doi.org/10.1029/2009PA001906

Petersen, S. V., & Schrag, D. P. (2015). Antarctic ice growth before and after the Eocene-Oligocene transition: New estimates from clumped isotope paleothermometry. *Paleoceanography*, *30*, 1305–1317. https://doi.org/10.1002/2014PA002769

Plancq, J., Mattioli, E., Pittet, B., Simon, L., & Grossi, V. (2014). Productivity and sea-surface temperature changes recorded during the late Eocene–early Oligocene at DSDP Site 511 (South Atlantic). *Palaeogeography, Palaeoclimatology, Palaeoecology*, *407*, 34–44.

Pusz, A. E., Thunell, R. C., & Miller, K. G. (2011). Deep water temperature, carbonate ion, and ice volume changes across the Eocene-Oligocene climate transition. *Paleoceanography*, *26*, PA2205. https://doi.org/10.1029/2010PA001950

Rongstad, B. L., Marchitto, T. M., & Herguera, J. C. (2017). Understanding the effects of dissolution on the Mg/Ca paleothermometer in planktic foraminifera: Evidence from a novel individual foraminifera method. *Paleoceanography*, *32*, 1386–1402. https://doi.org/10.1002/2017PA003179

Sadekov, A., Eggins, S. M., De Deckker, P., & Kroon, D. (2008). Uncertainties in seawater thermometry deriving from intratest and intertest Mg/Ca variability in Globigerinoides ruber. *Paleoceanography*, *23*, PA1215. https://doi.org/10.1029/2007PA001452

Sadekov, A., Eggins, S. M., De Deckker, P., Ninnemann, U., Kuhnt, W., & Bassinot, F. (2009). Surface and subsurface seawater temperature reconstruction using Mg/Ca microanalysis of planktonic foraminifera *Globigerinoides ruber*, *Globigerinoides sacculifer*, and *Pulleniatina obliquiloculata*. *Paleoceanography*, *24*, PA3201. https://doi.org/10.1029/2008PA001664

Sexton, P. F., Wilson, P. A., & Pearson, P. N. (2006). Microstructural and geochemical perspectives on planktic foraminiferal preservation: "Glassy" versus "Frosty". *Geochemistry Geophysics Geosystems*, *7*, Q12P19. https://doi.org/10.1029/2006GC001291

Shackleton, N. J., & Kennett, J. P. (1975). Late Cenozoic oxygen and carbon isotopic changes at DSDP Site 284: Implications for glacial history of the Northern Hemisphere and Antarctica. *Initial Reports of the Deep Sea Drilling Project*, *29*, 801–807.

Wade, B. S., Houben, A. J. P., Quaijtaal, W., Schouten, S., Rosenthal, Y., Miller, K. G., et al. (2012). Multiproxy record of abrupt sea-surface cooling across the Eocene-Oligocene transition in the Gulf of Mexico. *Geology*, *40*(2), 159–162. https://doi.org/10.1130/G32577.1

Waghorn, D. B. (1989). Middle Tertiary calcareous nannofossils from Aire District, Victoria - A comparison with equivalent assemblages in South Australia and New Zealand. *Marine Micropaleontology*, *14*, 237–255.

Wilson, P. A., & Norris, R. D. (2001). Warm tropical ocean surface and global anoxia during the mid-Cretaceous period. *Nature*, *412*(6845), 425–429. https://doi.org/10.1038/35086553

Wilson, P. A., & Opdyke, B. N. (1996). Equatorial sea-surface temperatures for the Maastrichtian revealed through remarkable preservation of metastable carbonate. *Geology*, *24*(6), 555–558.

Zachos, J. C., Opdyke, B. N., Quinn, T. M., Jones, C. E., & Halliday, A. N. (1999). Eocene-Oligocene climate and seawater 87Sr/86Sr: Is there a link? *Chemical Geology*, *161*, 165–180.

Zachos, J. C., Quinn, T. M., & Salamy, K. (1996). High resolution (104 yr) deep-sea foraminiferal stable isotope time series. *Paleoceanography*, *11*, 251–266.

Zachos, J. C., Stott, L. D., & Lohmann, K. C. (1994). Evolution of early Cenozoic marine temperatures. *Paleoceanography*, *9*, 353–387.

References From the Supporting Information

Carter, A. N. (1958). Tertiary foraminifera from the Aire District, Victoria. Geological Survey of Victoria, Melbourne.

Carter, A. N. (1964). Tertiary foraminifera from Gippsland, Victoria and their stratigraphical significance. Geological Survey of Victoria, Melbourne.

de Hornibrook, N. B. (1961). *Tertiary Foraminifera from Oamaru District (NZ)*. New Zealand: New Zealand Geological Survey.

Eggins, S., De Deckker, P., & Marshall, J. (2003). Mg/Ca variation in planktonic foraminifera tests: Implications for reconstructing palaeo-seawater temperature and habitat migration. *Earth and Planetary Science Letters*, *212*, 291–306.

Fisher, R. A. (1953). Dispersion on a sphere. *Proceedings of the Royal Society of London A: Mathematical, Physical and Engineering Sciences*, *217*, 295–305.

Heslop, D., & Roberts, A. P. (2012). Estimation of significance levels and confidence intervals for first-order reversal curve distributions. *Geochemistry, Geophysics, Geosystems*, *13*, Q12Z40. https://doi.org/10.1029/2012GC004115

Kirschvink, J. L. (1980). The least squares line and plane and the analysis of palaeomagnetic data. *Geophysical Journal of the Royal Astronomical Society*, *62*, 699–718.

Lurcock, P. C., & Wilson, G. S. (2012). PuffinPlot: A versatile, user-friendly program for paleomagnetic analysis. *Geochemistry, Geophysics, Geosystems*, *13*, Q06Z45. https://doi.org/10.1029/2012GC004098

Pike, C. R., Roberts, A. P., & Verosub, K. L. (1999). Characterizing interactions in fine magnetic particle systems using first order reversal curves. *Journal of Applied Physics*, *85*, 6660–6667.

Pike, C. R., Roberts, A. P., & Verosub, K. L. (2001). First-order reversal curve diagrams and thermal relaxation effects in magnetic particles. *Geophysical Journal International*, *145*, 721–730.

Roberts, A. P. (2015). Magnetic mineral diagenesis. *Earth-Science Reviews*, *151*, 1–47.

Roberts, A. P., Heslop, D., Zhao, X., & Pike, C. R. (2014). Understanding fine magnetic particle systems through use of first-order reversal curve diagrams. *Reviews of Geophysics*, *52*, 557–602. https://doi.org/10.1002/2014RG000462

Santrock, J., Studley, S. A., & Hayes, J. M. (1985). Isotopic analyses based on the mass-spectrum of carbon-dioxide. *Analytical Chemistry*, *57*(7), 1444–1448. https://doi.org/10.1021/ac00284a060

Zijderveld, J. D. A. (1967). AC demagnetisation of rocks: Analysis of results. In D. W. Collinson, K. M. Creer, & S. K. Runcorn (Eds.), *Methods in Palaeomagnetism* (pp. 254–296). Amsterdam: Elsevier.